

Long-range electron transport in a self-organizing n-type organic material

V. Duzhko* and K.D. Singer

Department of Physics, Case Western Reserve University, Cleveland, Ohio 44106, USA

E. Aqad, M. Peterca, and V. Percec

Department of Chemistry, University of Pennsylvania, Philadelphia, Pennsylvania 19104, USA

Abstract

Nondispersive time-of-flight electron transport has been observed in a self-organizing perylene diimide derivative, (3,4,5Pr)12G1-3-perylenetetracarboxyl-diimide, yielding long-range transport mechanisms that correlate with molecular packing in several structural phases. The consistency of temperature- and electric-field-dependences of electron mobility in the isotropic and columnar Φ_{h1} phases with static rather than dynamic disorder formalisms provides a link between molecular packing, energetic and positional disorder, and magnitudes of mobility.

* *Corresponding author:*
Volodymyr Duzhko
Department of Physics,
Case Western Reserve University
10900 Euclid Ave, Cleveland, OH 44106
Phone: 1 (216) 368 4369; Fax: 1 (216) 368 4671
E-mail: volodymyr.duzhko@case.edu

Self-organizing organic materials such as certain regioregular polymers,^{1,2} liquid crystals^{3,4} and liquid-crystal-templated crystals⁵ lead to superior performance in organic field-effect-transistors,^{1,5} photovoltaic cells,^{2,3} etc. making them candidates for the next generation of cost-effective optoelectronic materials. Molecular self-organization in soft condensed phases enables creation of novel functional materials with unique properties.⁶ Further, self-assembly of organic nanostructures in solution^{7,8} leads to novel architectural concepts in optoelectronic applications.⁹

Discotic (disc-like) molecules self-assemble into well-ordered columnar stacks with overlapping core electronic orbitals providing quasi-one-dimensional charge carrier transport.¹⁰ The relative stack core orientation and molecular reorganization energies involving charged-neutral state transitions contribute to a molecular-scale picture of charge transfer processes.¹¹ The magnitudes of short-range mobilities in self-organized discotic phases^{12,13} approach the range typical of well-ordered oligoacene crystals. The mobilities at longer length- and time-scales, however, remain significantly smaller.¹⁴ Morphological imperfections, *i.e.* limited coherence length in the molecular stacks, grain boundaries, misalignment of columns between the electrodes and impurities, contribute to reduced long-range mobilities and increased transport-path dispersion, impeding mobility measurements. Previous efforts to understand the long-range^{4,14,15} charge carrier transport mechanisms with specific temperature- and electric-field-independent mobilities, and to correlate the magnitudes of mobilities with structural properties have focused on the hole-conducting (p-type) materials. Transport properties of electron-conducting (n-type) materials, such as the often studied perylene diimides, are known to degrade in air as was well-documented for the vacuum-sublimated thin crystalline films.^{5,16,17} Stringent requirements for material purity¹⁸ and processing in an inert atmosphere have prevented the measurement of the long-range electron mobilities in self-organizing n-type organic materials.

In this Letter, we describe non-dispersive long-range electron transport in a self-organizing n-type organic material, (3,4,5Pr)12G1-3-perylenetetracarboxyldiimide, as measured by the time-of-flight (TOF) technique. It is shown that mobilities increase with the improved molecular packing in the accessible self-organized phases. The consistency of the temperature- and electric-field-dependences of mobility with free-carrier hopping has enabled correlation of molecular packing with energy distribution and positional disorder of hopping sites, with magnitudes of electron mobility. This provided us with the tool for similar studies in a number of self-organizing derivatives with systematic variations in coherence length of molecular stacks and degree of chirality.¹⁹

The perylene diimide derivative, (3,4,5Pr)12G1-3-perylenetetracarboxyldiimide (PTCBI, inset to Fig.1a), was purified using several steps including column chromatography and multiple precipitations from methanol. Purification was monitored by observing the width of the phase transition to isotropic phase in the differential scanning calorimetry (DSC) traces. The DSC (see Fig. S1 in Ref. 20) and X-ray diffraction data reveal the existence of several structural phases with different molecular packing: a disordered isotropic phase (*I*) above 125 °C, a columnar mesophase Φ_{h2} (125 °C – 80 °C) and a more ordered low temperature phase Φ_{h1} (80 °C – -20 °C). A detailed analysis of the nature and structure of the phases is underway and will be published later.¹⁹

Samples for the TOF measurements were constructed in a sandwich geometry using ITO-coated glass substrates, silica beads of 11 μm diameter separating the substrates, with spring clips holding the structure together. The cell thickness was determined by interference in a UV-vis spectrophotometer. The ITO cells were then filled by PTCBI at 135 °C by capillary forces and cooled down to 25 °C at a rate of 0.2 °C. The inset to Fig. 1b shows a typical polarized microscopy image of PTCBI film. Black areas indicate self-organized domains with homeotropic alignment and in-plane size of $\sim 100 \mu\text{m}$. This size domain, much larger than the

film thickness, indicates the absence of interfaces along the transport path between the electrodes. The precautions taken to eliminate the parasitic dark currents, to process the material in inert atmosphere as well as to monitor any possible degradation upon exposure to air were described elsewhere.²⁰ The entire fabrication procedure followed was critical to our ability to observe well-defined transit times in TOF transients.

A conventional TOF set-up was used to measure photocurrent transients at various temperatures.⁴ Charge carriers were excited by a 3.6 ns Q-switched Nd:YAG-based laser (Surelite) that was frequency doubled and frequency shifted using a H₂ stimulated Raman shifter. The absorption of the third anti-Stokes component at 320 nm in the liquid crystal results in creation of a photo-generated narrow sheet of electron-hole pairs near the illuminated electrode that is much thinner than the internal cell thickness. Only the electron-related transit times for a respective bias polarity could be measured and will be discussed. All TOF measurements were done in air shortly after removal from inert atmosphere; however the data remain reproducible during the observation period of four months.

Typical photocurrent transients measured in PTCBI derivative at 20 °C for different applied bias voltages (a) or at 200 V for different structural phases (b,c) are shown in Fig. 1. Immediately after the laser pulse, the photocurrent at 20 °C monotonically decreases due to trapping of photo-excited electrons on their way toward the opposite electrode, followed by a rapid change of slope at transit time τ_{tr} . The shift of τ_{tr} with the applied bias (V) indicates the passage of electrons through the entire thickness of the cell (L) and enables determination of the electron mobility as $\mu = L^2/V\tau_{tr}$. Changes in photocurrent transient shapes are observed at the various phase transitions. Above 20 °C, non-dispersive transport is observed, i.e. a current transient shape characteristic of transit times distributed according to Gaussian statistical broadening of the drifting charge sheet and with τ_{tr} is well-defined in a linear plot. Above 100 °C, a somewhat dispersive transient, however with reduced shallow trapping effects, is

observed, and above 125 °C, the photocurrent transients characterize strongly dispersive transport.

The dependence of electron mobility on temperature (Fig. 2a) and electric field (Fig. 3) were measured in order to identify the charge carrier transport mechanisms in the various structural phases of PTCBI. The carrier mobility undergoes a step-like increase at the phase transitions, $I \rightarrow \Phi_{h2}$ (125 °C) and $\Phi_{h2} \rightarrow \Phi_{h1}$ (80 °C), reflecting the improving molecular packing as the temperature is reduced. We now analyze the temperature and electric-field dependence of mobility in I and Φ_{h1} mesophases in terms of two charge transport models considering static or dynamic disorder in the system, namely the hopping of free carriers over the sites with a Gaussian energy and distance distributions²¹ or uncorrelated hopping of small polarons²² and neglecting any temperature-induced structural changes *within* the phases.

The mobility for free carrier hopping over disordered sites is given by²¹

$$\mu = \mu_0 \exp\left[-\left(\frac{2}{3} \frac{\sigma}{kT}\right)^2\right] \exp\left[C \left(\left(\frac{\sigma}{kT}\right)^2 - \Sigma^2\right) E^{1/2}\right] \quad (1)$$

where, σ is the energy width of the hopping site manifold, Σ - a parameter that describes the degree of positional disorder, μ_0 - the mobility prefactor, and $C = 2.9 \times 10^{-4} \text{ (cm/V)}^{1/2}$.

The mobility for uncorrelated small-polaron hopping model is given by²²

$$\mu = \mu_0 \exp\left(-\frac{1}{2\Delta_p} - J\right) / kT \quad (2a)$$

and its electric field dependence by²³

$$\mu \propto E^{-1} \sinh(eEa / 2kT) \quad (2b)$$

where μ_0 is the mobility prefactor, a - inter-site distance, Δ_p - the polaron binding energy, J - the nearest neighbor electron transfer integral, with $J \ll \Delta_p$ if polaron delocalization phenomena are neglected.

The fitting curves (lines) of the measured temperature dependence of mobility (symbols) to Eq.(1) and Eq. (2a) are shown in Fig. 2b and Fig. 2c, respectively. The fitting parameters of the disordered hopping formalism in **I** phase are $\mu_0 = 0.034 \text{ cm}^2/\text{Vs}$ and $\sigma = 0.159 \text{ eV}$, and in Φ_{hI} phase are $\mu_0 = 0.06 \text{ cm}^2/\text{Vs}$ and $\sigma = 0.104 \text{ eV}$. The values of μ_0 , σ , as well as Σ (see discussion below) in **I** phase are similar to the typical values in polymers.²¹ The larger σ and smaller μ_0 in **I** as compared to Φ_{hI} are both consistent with improved molecular packing in the latter phase. Additionally, the prefactor mobility μ_0 is in agreement with the short range mobility of $0.01 \text{ cm}^2/\text{Vs}$ for similar self-organizing PTCBIs.^{24,25} The deduced long-range TOF mobility is about two orders of magnitude smaller than the short-range one. This difference suggests that the macroscopic morphology factors limit the long-range mobility of electrons by introducing the energetic and positional disorder of transport sites. Though the experimental curves seem to be well-described by the small polaron hopping model, the extracted polaron binding energies Δ_p of 1.23 eV and 0.7 eV in **I** and Φ_{hI} , respectively, as well as the larger μ_0 of $155 \text{ cm}^2/\text{Vs}$ in the disordered phase as compared to μ_0 of $33 \text{ cm}^2/\text{Vs}$ in the more ordered Φ_{hI} phase are difficult to justify. These Δ_p would result in reorganization energies λ ($\mu \propto \exp(-\lambda/4kT)$), being significantly larger than the typical reorganization energies for this class of materials.²⁶

Figure 3 shows the electric field (**E**) dependence of electron mobility in Φ_{h2} (a), and in Φ_{hI} at various temperatures (b) with their fits with Eq.1. The weak electric field dependence in the isotropic phase ($>125 \text{ }^\circ\text{C}$) could not be reliably measured due to the somewhat dispersive photocurrent transients giving inadequately determined transit times. From the two-dimensional set of $\mu(\mathbf{E}, T)$ data, the values of $C=(8.8\pm 2.2)\times 10^{-4} \text{ (cm/V)}^{1/2}$ and $\Sigma=3.35\pm 0.6$ were determined. The latter parameter gives a degree of positional disorder in the system under study. The deviation of the experimental data from the linear dependence at

small electric fields (Eq. 2b) in the given coordinates in Fig. 3c is further evidence for the inconsistency of a small polaron description for our system. Therefore, static energetic and positional disorder are the major factors defining the magnitude of electron mobility in I and Φ_{h1} phases. Though the polaronic description alone is not consistent with the data, some polaronic contribution to the nature of charge carriers can not be excluded.

In conclusion, the mechanisms of long-range charge carrier transport have been accessed in several self-organized phases of n-type organic material by the TOF technique. The magnitude, temperature- and electric-field dependences of electron mobility, as well as the shape of photocurrent transients reflect an improved molecular packing upon phase transitions from I to Φ_{h2} , and to Φ_{h1} . The temperature- and electric-field-independent electron mobility, and reduced trapping effects that are also inherent to hole transport in discotic liquid crystals,¹⁴ show similar nature of two types of charge carriers. Finally, the studied material demonstrated well-reproducible and stable operation in air for several months after fabrication into sandwich cells.

References

- ¹ I. McCulloch, M. Heeney, C. Bailey, K. Genevicius, I. MacDonald, M. Shkunov, D. Sparrowe, S. Tierney, R. Wagner, W. Zhang, M.L. Chabinyc, R.J. Kline, M.D. McGehee, and M.F. Toney, *Nature Materials* **5**, 328 (2006).
- ² Y. Kim, S. Cook, S.M. Tuladhar, S.A. Choulis, J. Nelson, J.R. Durrant, D.D.C. Bradley, M. Giles, I. McCulloch, C.-S. Ha, and M. Ree, *Nature Materials* **5**, 197 (2006).
- ³ L. Schmidt-Mende, A. Fechtenkoetter, K. Muellen, E. Moons, R.H. Friend, J.D. MacKenzie, *Science* **293**, 1119 (2001).
- ⁴ V. Duzhko, A. Semyonov, R.J. Twieg, and K.D. Singer, *Phys. Rev. B* **73**, 064201 (2006).
- ⁵ An improved degree of order can be achieved in crystalline films, if the constituent molecules are functionalized to be capable of forming liquid crystalline mesophases, by heating the films to the temperatures above the liquid crystal phase transition and subsequent controlled cooling. An example of this approach can be found in S. Tatemichi, M. Ichikawa, T. Koyama, Y. Taniguchi, *Appl. Phys. Lett.* **89**, 112108 (2006).
- ⁶ V. Percec, M. Glodde, T. K. Bera, Y. Miura, I. Shiyanovskaya, K. D. Singer, V. S. K. Balagurusamy, P. A. Heiney, I. Schnell, A. Rapp, H.-W. Spiess, S. D. Hudsonk & H. Duan, *Nature* **417**, 384 (2002).
- ⁷ V. Duzhko and K.D. Singer, *J. Phys. Chem. C* **111**, 27 (2007).
- ⁸ V. Duzhko, H. Shi, K.D. Singer, A.N. Semyonov, R.J. Twieg, *Langmuir* **22**, 7947 (2006).
- ⁹ Y. Yamamoto, T. Fukushima, Y. Suna, N. Ishii, A. Saeki, S. Seki, S. Tagawa, M. Taniguchi, T. Kawai, T. Aida, *Science* **314**, 1761 (2006).
- ¹⁰ D. Adam, F. Closs, T. Frey, D. Funhoff, D. Haarer, H. Ringsdorf, P. Schuhmacher, and K. Siemensmeyer, *Phys. Rev. Lett.* **70**, 457 (1993).
- ¹¹ V. Lemaire, D. A. da Silva Filho, V. Coropceanu, M. Lehmann, Y. Geerts, J. Piris, M. G. Debije, A. M. van de Craats, K. Senthilkumar, L. D. A Siebbeles, J. M. Warman, J.-L. Bredas, and J. Cornil, *J. Am. Chem. Soc.* **126**, 3271 (2004).
- ¹² A.M. van de Craats, J.M. Warman, A. Fechtenkoetter, J.D. Brand, M.A. Harbison, and K. Muellen, *Adv. Mater.* **11**, 1469 (1999).
- ¹³ Z. Chen, V. Stepanenko, V. Dehm, P. Prins, L.D.A. Siebbeles, J. Seibt, P. Marquetand, V. Engel, and F. Würthner, *Chem. Eur. J.* **13**, 436 (2007).
- ¹⁴ R.J. Bushby, O.R. Lozman, *Curr. Op. Sol. St. Mater. Sci.* **6**, 569 (2002).

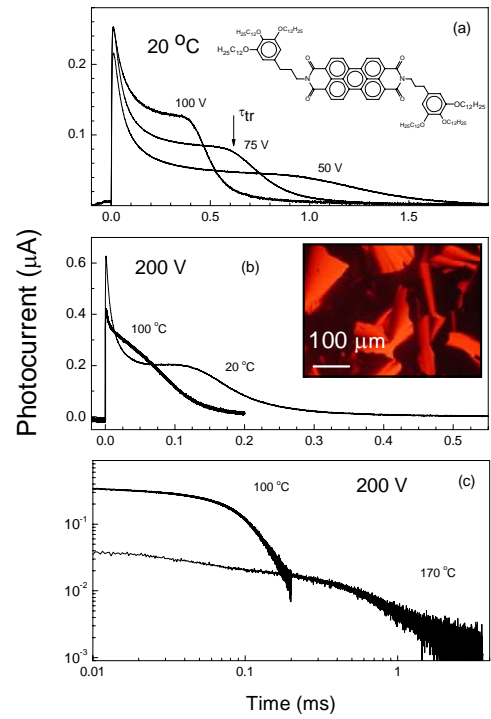
- ¹⁵ L.J. Lever, R.W. Kelsall, and R.J. Bushby, *Phys. Rev. B* **72**, 035130 (2005).
- ¹⁶ P.R. Malenfant, C.D. Dimitrakopoulos, J.D. Gelorme, L.L. Kosbar, T.O. Graham, *Appl. Phys. Lett.* **80**, 2517 (2002).
- ¹⁷ R.J. Chesterfield, J.C. McKeen, C.R. Newman, P.C. Ewbank, D.A. da Silva Filho, J.-L. Bredas, L.L. Miller, K.R. Mann and C.D. Frisbie, *J. Phys. Chem. B* **108**, 19281 (2004).
- ¹⁸ H. Iino, J.-i. Hanna, D. Haarer, *Phys. Rev. B* **72**, 193203 (2005).
- ¹⁹ V. Percec, E.Aqad, M. Peterca, V. Duzhko, H. Shi, and K.D. Singer, in preparation.
- ²⁰ EPAPS document No. For more information on EPAPS, see <http://www.aip.org/pubserve/epaps.html>.
- ²¹ H. Bässler, *phys. stat. sol. (b)* **175**, 15 (1993).
- ²² T. Holstein, *Ann. Phys.* **8**, 325-389 (1959).
- ²³ R.A. Markus, *Ann. Rev. Phys. Chem.* **15**, 155 (1964).
- ²⁴ M.G. Debije, Z. Chen, J. Piris, R.B. Neder, M.M. Watson, K. Müllen, and F. Würthner, *J. Mater. Chem.* **15**, 1270 (2005).
- ²⁵ Z. An, J. Yu, S.C. Jones, S. Barlow, S. Yoo, B. Domercq, P. Prins, L.D.A. Siebbeles, B. Kippelen, and S.R. Marder, *Adv. Mater.* **17**, 2580 (2005).
- ²⁶ J.-L. Bredas, D. Beljonne, V. Coropceanu, and J. Cornil, *Chem. Rev.* **104**, 4971 (2004).

Figure captions

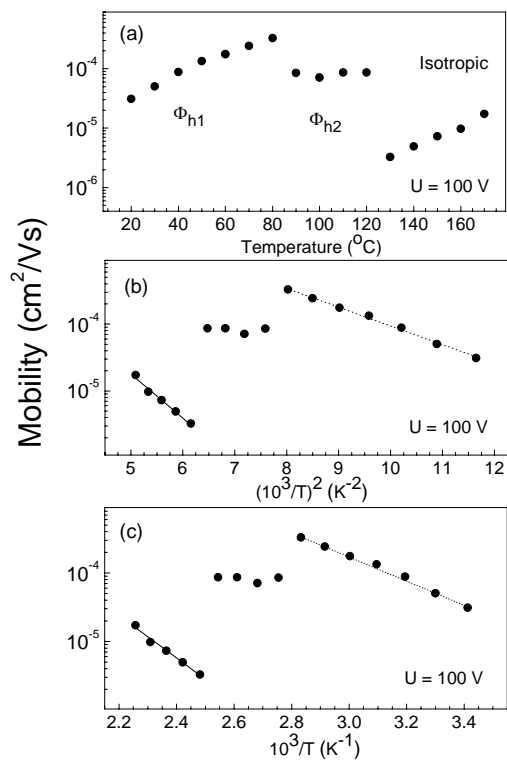
FIG. 1. (Color online) (a) Typical photocurrent transients in PTCBI derivative measured at 20 °C for various applied biases, and (b,c) at an applied bias of 100 V in different structural phases. The insets show (a) the chemical structure of PTCBI and (b) a polarized microscopy image of an 11 μm -thick film at 20 °C after cooling from the isotropic phase at a rate of 0.2 °/min.

FIG. 2. (a) Temperature dependence of electron mobility in PTCBI (symbols) at an applied bias of 100 V. The fits with Eq. (1) and Eq. (2a) are given for comparison in (b) and (c), respectively. Note the different scales.

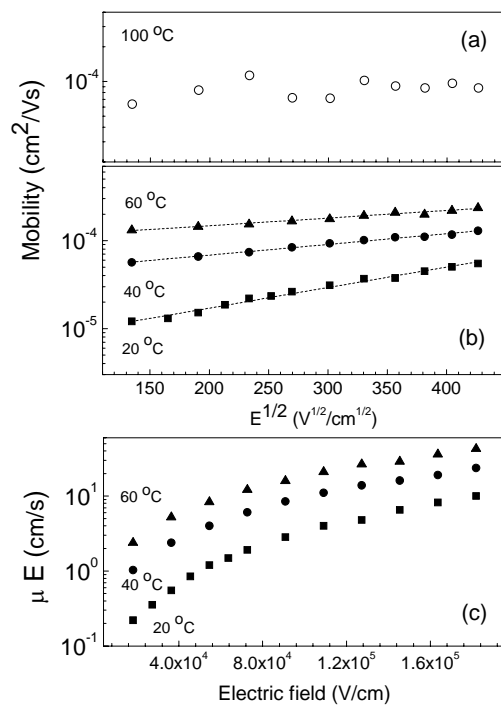
FIG. 3. Dependence of electron mobility (μ) on the electric field (E) in PTCBI (symbols) measured (a) at 100 C in Φ_{h2} phase, and (b,c) for a series of temperatures within Φ_{h1} phase. The fits (lines) of experimental data to Eq. (1) are shown for comparison.



Duzhko et al., Figure 1



Duzhko et al., Figure 2



Duzhko et al., Figure 3

Long-range electron transport in a self-organizing n-type organic material

V. Duzhko* and K.D. Singer

Department of Physics, Case Western Reserve University, Cleveland, Ohio 44106, USA

E. Aqad, M. Peterca, and V. Percec

Department of Chemistry, University of Pennsylvania, Philadelphia, Pennsylvania 19104, USA

Supplemental materials

1. Differential Scanning Calorimetry data

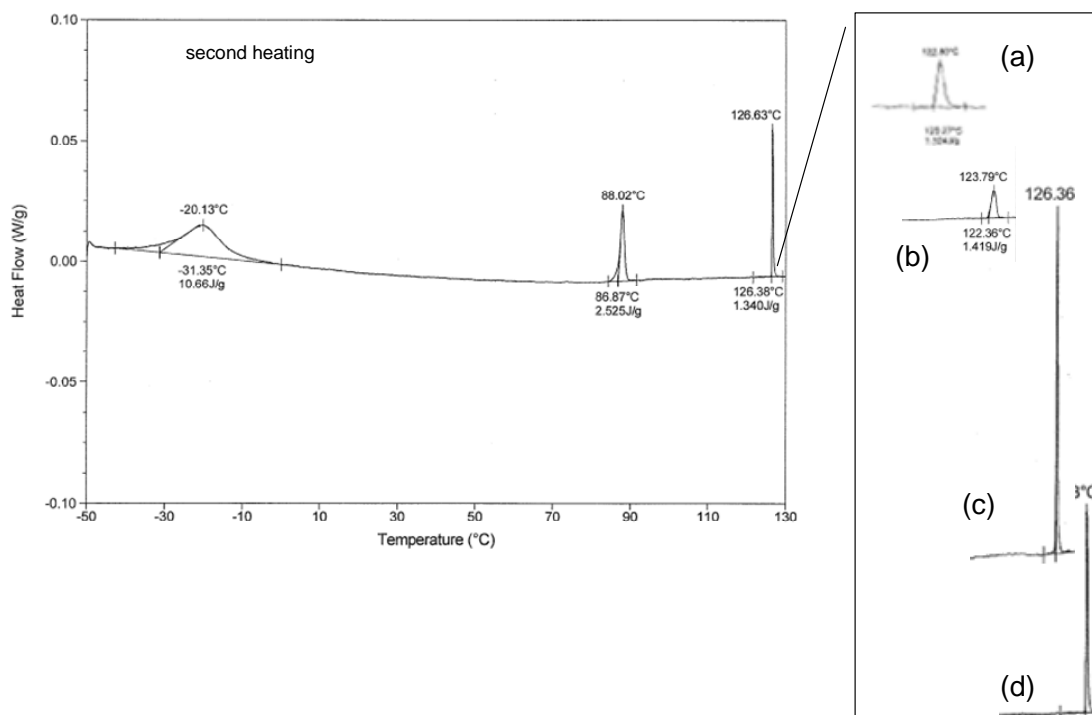


FIG. S1 Differential scanning calorimetry traces for PTCBI derivative measured at a rate of 10 °/min on second heating. The insets show the magnified peak at 126 °C before the purification by precipitation from methanol (a), after two (b), four (c) and five (d) cycles of precipitation. Narrowing of the peak suggests an improving purity of the powder.

2. Materials handling procedures and detailed sample fabrication

The PTCBI powders were either immediately stored in inert atmosphere after purification or evacuated for more than 5 days if they had been previously exposed to air. The empty ITO cells were baked for 2 hours at 130 °C before transferring warm into a glove box. Further fabrication steps were carried out in a glove box (N₂) and included filling PTCBI in its melted state at 135 °C into the ITO cell by capillary forces, uncontrolled cooling after removing the films from the hotplate, transferring the films into a vacuum cryostat that is then filled with N₂ gas, heating the films up to 135 °C and slowly cooling down to 25 °C at a rate of 0.2°/min. The short exposure of the completed cell in air for up to 2 min was found not to affect the results as the free surface is very small. Measurements of current-voltage characteristics in combination with the space-charge-limited-current technique were used to monitor the possible reduction of dark conductivity and consequently, charge carrier mobility upon exposure of samples to air. Unlike most observations of PTCBIs in the field effect transistor geometry, no reduction in conductivity or mobility was observed during the exposure of samples to air for up to ~2 hours of monitoring. Further, the complete agreement between measured TOF mobilities on heating and cooling after several hours of measurements, as well as the reproducibility of these measurements after 4 months of storage of a fabricated cell in air evidence against any storage-induced changes in charge carrier transport properties in cells of this material. We relate this stability to the favorable geometry of the *completed cell* having limited exposed surface area and thus much smaller free-surface-to-volume ratio.

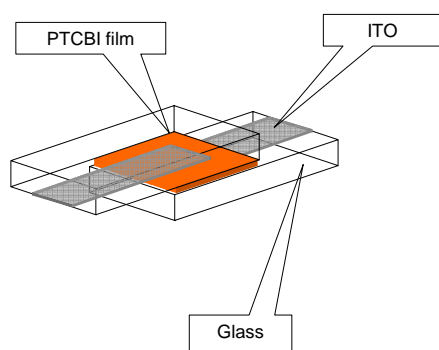


FIG. S2. Schematic geometry of a cell used in the time-of-flight, space-charge-limited-current and polarized microscopy measurements. The sandwich-type cell consists of a perylene diimide film in-between the two ITO electrodes. The electrode edges were etched by ~2 mm at three sides to remove the ITO layer. The active device area was ~5×5 mm².

3. Elimination of parasitic dark dc conductivity

The ITO substrates used for the time-of-flight measurements had 2 mm-wide strips etched at the edges of the ITO electrodes so that the electrode boundaries were within the film boundaries (Fig. S2). When the film boundary was inside of the electrode boundary, an anomalous large current may flow across the free surface between the electrodes. This current could be ~ 3 orders of magnitude larger than the dark current through the bulk of PTCBI leading to misinterpretations in estimation of the space-charge-limited-current mobility.

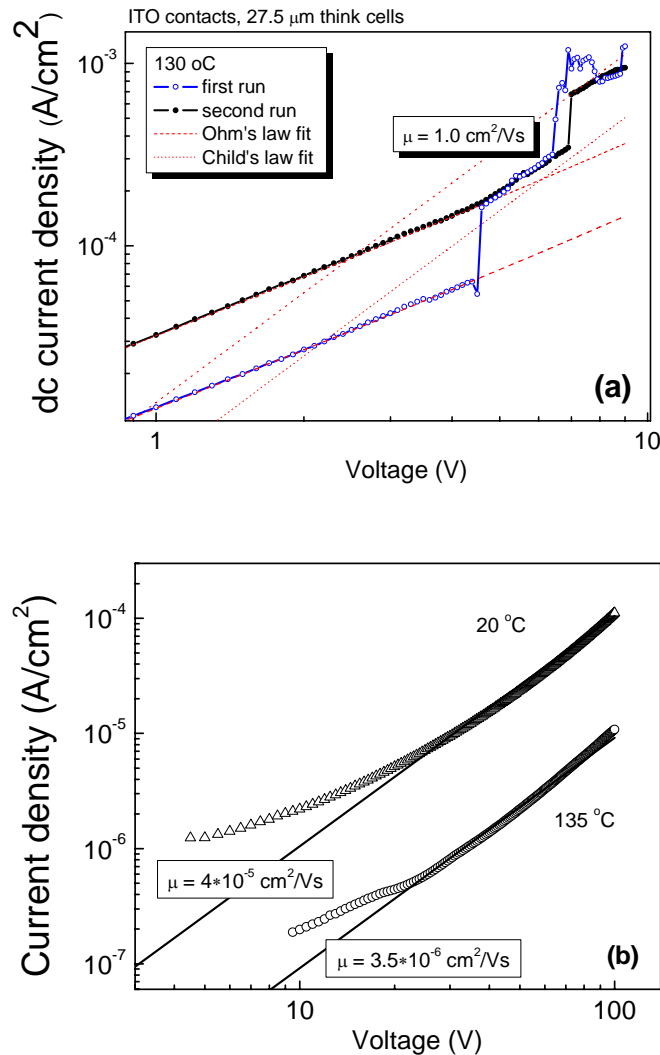


FIG. S3. Comparison of the current-voltage characteristics for the non-etched (top, 27.5 microns thick) and etched (bottom, 11 microns thick) cells of PTCBI derivative (see text above). Note, that the dc current is significantly larger for the non-etched cells.

Fitting of the experimental curves of Fig. S3a to Eq. (3) produces mobility of 1 cm²/Vs, while fitting of Fig. S3b produces mobility of 3.5×10⁻⁶ cm/Vs in the isotropic phase. While the latter mobility is in good agreement with the time-of-flight measurements and its magnitude changes in various phases accordingly to the shown TOF data, the former high dark current density is temperature-independent, purely reproducible from sample to sample and drops to the lower values (coincides with the etched cells one) after several runs. We associate this current with the parasitic surface conductivity through edges of the cells.

APPENDIX A. Space-charge-limited-current mobility

The charge carrier mobilities can be estimated from current-voltage characteristics measurements using the space-charge-limited-current regime.

Ohm's law with field-dependent mobility:

$$j(T, F) = en(T)\mu_0(T) \exp(\alpha(T)\sqrt{F}) F / L \quad (1)$$

Electric field-dependent mobility:

$$\mu(T, F) = \mu_0 \exp(\alpha\sqrt{F}) \quad (2)$$

where e is the elementary charge, n – density of intrinsic carriers, L – film thickness.

Child's law with field-dependent mobility:

$$j(T, F) = \frac{9}{8} \theta \varepsilon \varepsilon_0 \mu_0(T) \exp(\alpha(T)\sqrt{F}) F^2 / L^3 \quad (3)$$

where θ - is the contact injection efficiency, ε – dielectric constant